Received: 3 January 2021 | Revised: 20 April 2022 | Accepted: 6 June 2022

DOI: 10.1002/mp.15813

RESEARCH ARTICLE

MEDICAL PHYSICS

Electron backscattering for signal enhancement in a thin-film CdTe radiation detector

Fatemeh Akbari | **Diana Shvydka**

Department of Radiation Oncology, University of Toledo Health Science Campus, Toledo, Ohio, USA

Correspondence
Diana Shvydka, Department of Radiation Oncology, University of Toledo Health Science Campus, Mail Stop #1151, 3000 Arlington Avenue, Toledo, OH 43614, USA.
Email: Diana.Shvydka@utoledo.edu

Abstract

Background: Thin-film cadmium telluride (CdTe) offers high average electron density, direct detection configuration, and excellent radiation hardness, making it an attractive material for radiation detectors. Although a very thin detector provides capabilities to conduct high-resolution measurements in high-energy radiation fields, it is limited by a low signal, often boosted with a front metal converter enhancing X-ray absorption. An extension of this approach can be explored through the investigation of electron backscattering phenomenon, known to be highly dependent on the material atomic number *Z*. Adding an electron reflector in tandem with the back electrode is proposed to be utilized for the detector signal enhancement.

Purpose: We investigated the possibility of augmenting the fluence of electrons traversing CdTe thin film and thus increasing the detected signal pursuing two pathways: (1) adding a high-*Z* metal layer to the back of the detector surface, and (2) adding a top low-*Z* material to the detector layer to return its backscattered electrons. Copper (Cu) and lead (Pb) layers of varying thickness were investigated as potential metal back-reflectors, whereas polymethyl methacrylate (PMMA) water phantom material was tested as the top cover in multilayer detector structures.

Methods: The Monte Carlo (MC) radiation transport package MCNP5 was first used to model a basic multilayer structure of a CdTe-sensitive volume surrounded by PMMA, under a 6-MV photon beam. Addition of Cu or Pb back-reflectors allowed for the analysis of the signal enhancement and associated changes in Compton electrons fluence spectra. Related backscattering coefficients were then calculated using EGSnrc MC user-code for monoenergetic electron sources. Analytical functions were established to represent the best fitting curves to the simulation data. Finally, electron backscattering data was related to signal enhancement in the CdTe sensitive layer based on a semiquantitative approach.

Results: We studied multilayer detector structures, decoupling the effects of PMMA and the back-reflector metals, Cu or Pb, on electron backscattering for electron energy range of up to 500 keV or 1 MeV depending on the choice of metal. Adding a 100–200-μm-thick metal film below the detector sensitive volume increased the fraction of reflected electrons, especially in the low, 100–200 keV, energy range. The thickness dependence of backscattering coefficients from thin films exhibits saturations at values significantly exceeding the electron ranges. That effect was related to the large-angle electron scattering. A

detailed simulation of energy deposition revealed that the modified structures using Cu and Pb increased energy deposition by ~10% and 75%, respectively. We have also established a linear dependence between the energy deposition in the semiconductor layer and the fluence of backscattered electrons in the corresponding multilayer structure. The low-*Z* top layer in practically implemental thicknesses of tens of micrometers has a positive effect due to partial electron reflection back to the semiconductor layer.

Conclusions: Signal enhancement in a thin-film CdTe radiation detector could be achieved using electron backscattering from metal reflectors. The methodology explored here warrants further studies to quantify achievable signal enhancement for various thin films and other small sensitive volume detectors.

KEYWORDS
CdTe detector, electron backscattering, signal enhancement

1 | INTRODUCTION

Semiconductor materials offer the convenience of direct signal detection under high-energy photon beams, utilized in diagnostic radiology and radiation therapy. They are employed in both dosimetry and imaging, with the latter option necessitating large area devices, implemented with thin films. For historical reasons, the choice of commercially available materials is limited to amorphous silicon (a-Si), although manufacturing technology for better suited semiconductors, such as cadmium telluride (CdTe), have been firmly established in photovoltaic applications.[1] Compared to a-Si, thin-film CdTe offers superior efficiency with higher average electron density, direct detection configuration, and outstanding radiation hardness.[2,3] With a typical device thickness below 1 mm, low absorption efficiency in high-energy photon beams calls for signal boosting. One established approach is to use a 2–3-mm thick metal "converter" plate above the thin film,[2] where the plate increases photon interactions and thus an influx of secondary electrons reaching CdTe-sensitive volume. Here we propose an approach to further enhance the detectable signal with a use of metal back-reflectors, relying on a known phenomenon of electron backscattering.

When electron beam is directed onto the surface of a solid target, some electrons are turned back, emerging from the surface, due to elastic and inelastic collisions with the atomic electrons and nuclei of the target medium. This process is often characterized in terms of the backscattering coefficient (η), defined as the ratio of the number of backscattered electrons to the total number of the incident electrons. The electron backscattering is of great interest in numerous applications such as scanning electron microscopy, electron microlithography, Auger electron spectroscopy, and studies of radiation damage. The phenomenon is also important in medical physics for the purpose of accurate assessment of dose deposited around inhomogeneities where backscattering alters the spatial energy distribution pattern.

Electron backscattering from bulk specimens, thin films, and their combinations has been a subject of many studies. Several attempts have been made to describe the electron backscattering process analytically by a simple theory.[4–9] In some applications, single scattering processes are insufficient to characterize electron backscattering. Existing multiple scattering theories, on the other hand, usually only describe a few limiting conditions or are difficult to assess. Most of the information comes from the experimental data, covering a wide range of incident angles and energies, target samples, and experimental geometries.[10–12] Most of these studies have been conducted for incident electron energies below 140 keV,[8, 10, 12–14] a few at high energies ($E > 1$ MeV).[11, 13, 15] Little data exists in the intermediate range (0.1 MeV $< E <$ 1 MeV),[15–17] which can be important for various spectroscopic applications, as well as in measurements and calculations of radiation fields in radiation therapy. Furthermore, electron backscattering coefficients have been obtained with Monte Carlo (MC) simulations using different codes, including MCNP, GEANT, EGSnrc, and CASINO[13–15, 17–30]; here the typical approach is to calculate the fraction of electrons scattered from a sample surface and returned into vacuum. The published data is usually described with empirical fitting functions, which are difficult to generalize to arbitrary targets, especially in multilayered structures.

The main purpose of this study was to explore the potential of modifying electron spectrum and boosting signal in a semiconductor radiation dosimeter utilizing electron backscattering. We conducted MC simulations of multilayer structures based on CdTe in combination with two significantly different metal back-reflectors, copper (Cu), and lead (Pb). The former option was selected due to its ubiquitous use in electronic circuits, whereas the latter offers high backscattering coefficient owing to its high atomic number.[4] A back-reflector

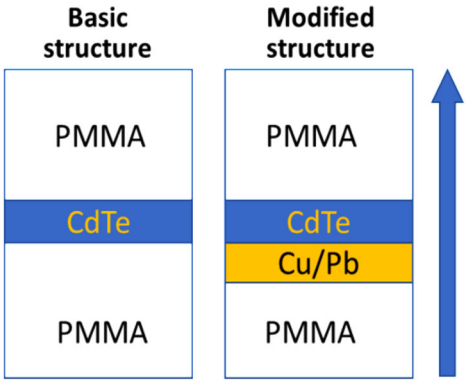

FIGURE 1 Schematic representation of the modeled detector design: basic structure and modified structure, including back reflector (not to scale). The arrow represents the direction of "backscattered" electrons.

can be incorporated as a separate layer placed below the detector. Alternatively, it can be technologically advantageous to attach it (e.g., via direct deposition) directly to the functional electrode, making the total electrode/reflector tandem 100–200-μm thick,[31] as dictated by the average secondary electron ranges. The effect of polymethyl methacrylate (PMMA), which is a water-equivalent material often used for detector encapsulation, is also investigated as a part of the detector design. Starting with a photon source modeling and establishing relevant parameters for the generated secondary electrons, we investigate the basic and modified structures under a set of monoenergetic electron sources. Finally, analytical functions that represent the best fitting curves to the simulated data were established. By decoupling the effects of PMMA and the back-reflector metals on CdTe backscattering properties, we can offer a general description of the multilayered detector properties without the need of simulating all conceivable layer configurations. Our approach can be generalized at least semiquantitatively to alternative semiconductors and back-reflectors.

2 | MATERIALS AND METHODS

2.1 | Detector design

MC simulations (MCNP5 package[32]) were conducted first to model a basic multilayered structure, including a CdTe-sensitive volume under 6-MV photon beam of a Varian linac.[33] The basic structure was then modified by the addition of a metal back-reflector serving to increase its detected signal. Schematic representation of the modeled detector design is shown in Figure 1, where the arrow on the right represents the direction of "backscattered" electrons, defined as any scattered or secondary electrons moving in the direction toward the primary source.

The CdTe of 30- and 300-μm thickness was simulated in combination with copper and lead, with surrounding a phantom-equivalent PMMA layer. For 6-MV photons, deposited energy "builds up" to an equilibrium value over a thickness range of ~1.5 cm. Thus, in addition to serving as a detector encapsulating layer, the PMMA layer in our structure also performed that function. Photon interactions set secondary (Compton) electrons in motion, and these electrons deposit their energy (dose) within the detector sensitive volume. Photon simulations were used to look at the generated secondary electron energy spectra at the interfaces among PMMA, semiconductor, and metal reflectors. They informed the next step of MC simulations under monoenergetic electron sources, defining the range of energy for backscattered electron fluence calculations.

The saturation thickness for which backscattered fraction becomes maximum (it is about the half of electron range for a specific energy) was used as the optimum thickness of the metal back-reflector layer. Range of electrons of different energies in materials of interest and properties of the materials are provided in Table 1. In all the simulations, we set cutoff energies to 10 keV for electrons and photons, with coherent, photonuclear, and Doppler interactions turned off, but Bremsstrahlung included. The number of particles crossing a surface was calculated using F1 tally (surface current) and cosine binning to distinguish between forward and backscattered particles. *F8 energy deposition tally was used to acquire relative signal in studied structures; the tally value was divided by the mass of the tally cell to obtain the energy deposition per unit mass of the detector sensitive volume. Photon histories of 3×10^8 were followed to achieve statistical errors less than 1%.

2.2 | Electron backscattering

Ali and Rogers[18] developed and made available a customized EGSnrc MC user-code for backscattering coefficient calculations. As the code conveniently provides backscattering coefficient value η for a customizable structure, it was utilized in this work to obtain most of data. The code simulates an electron or positron beam incident on a sample, which may be a thin film, a stack of films, or a bulk target considered infinite if its thickness is larger than the range of incident charged particles in the sample. The materials can be elements, mixtures, or compounds. The code validation against experimental data from 20 separate published experiments encompassing 35 distinct elements, electron and positron backscattering, normal and oblique incidence, confirmed the simulation results to be within 4%.[18] Although accurate charged particle backscattering simulation could be challenging for both the EGSnrc and MCNP codes that use the condensed history algorithm,

TABLE 1 Summary of modeled material properties: density, mean atomic number (Z), and the range of electrons (in μm) for different energies

Material	Density (g/cm^3)	Atomic number	E (keV)							
			20	50	100	150	200	300	500	700
PMMA	1.18	6	7	37	124	243	387	727	1525	2403
CdTe	6.20	52	3	15	46	88	138	254	519	802
Cu	8.96	29	2	8	25	48	76	140	292	456
Pb	11.35	82	2	9	27	52	81	147	296	454

Abbreviation: CdTe, cadmium telluride; PMMA, polymethyl methacrylate.

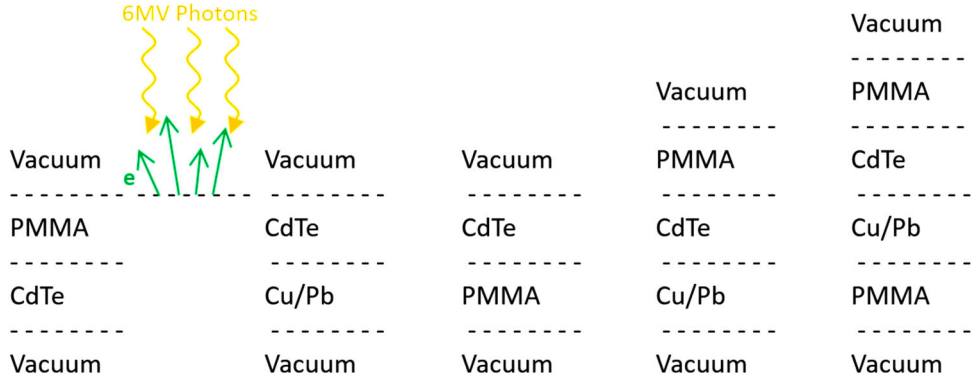

FIGURE 2 Simulations geometries used to calculate η at the first interface (top dashed line). Wavy arrows show the direction of incident 6-MV photon beam, and straight arrows show the backscattered electrons.

it has been shown that the implementation of this technique in the EGSnrc code yields results that are step-size independent and agree with single scattering (condensed) calculations within less than 0.1% for low energies.[34]

In this work, η was calculated for CdTe with added Pb or Cu reflector layer of varying thickness, 20–200 μm, and a top layer of PMMA of 1–50-μm thickness. The model comprised a pencil beam of monoenergetic charged particles incident normally on a thin-film sample or a stack of films, surrounded by vacuum. The geometry of each simulated structure is depicted in Figure 2. Backscattered charged particles were tallied as they crossed from the sample medium back to the vacuum. The values of electron and photon transport cutoff used in the simulations were 512 and 1 keV, respectively. For electrons, this value corresponds to a kinetic energy of 1 keV. A total of 5×10^4 electron histories were run; the maximum uncertainty in MC calculations of η values and energy spectra were 1% or lower.

The first step in our electron transport modeling involved the verification of the appropriateness of MC packages used for thin-film simulations, in a view of their use of condensed history algorithm. In MCNP, this approximation is defined by a parameter called DRANGE, which is the size of an energy step in g/cm^2. It is further divided into a number of substeps empirically determined to be in the range of values between 2 and 15, depending only on the average atomic number of the material.[32] A rule of thumb for the appropriate number is to ensure that electrons make at least 10 substeps in any material relevant to the transport problem; thus, the size of a substep should be compared to the smallest material dimension. Our problem geometry did comply with this rule; additionally, we verified that setting this parameter to its maximum value of 15 had virtually no effect on the results of our simulations.

Backscattering coefficient was calculated as the ratio among the total number of electrons reflected from the first non-vacuum layer and those entering the top layer. Electron backscattering coefficients obtained by the EGSnrc user-code were also verified against MCNP simulations, utilized to acquire the data not available from the EGSnrc user code. The change in electron backscatter and forward fluence was also investigated.

In order to obtain the value of η for the arbitrary target thickness combined with a metal back-reflector or surrounded with a PMMA layer, and for the incident kinetic energy E of the electrons, it would be convenient to derive an equation that well reproduces the most probable values given by the existing data. Therefore, the best fit for energy-dependent backscattering coefficients, characterized with the least R-square value, were also obtained for all structures for prognostic purposes.

2.3 | Estimate of signal enhancement based on the electron backscattering

Backscattering coefficients obtained for modified structures with back-reflectors were used for a semiqualitative estimate of signal enhancement in the CdTe sensitive layer. Specifically, increase in the reflection coefficient evaluated at the top of CdTe is indicative of additional traversing of the detector layer by electrons reflected from its bottom interface with metal. These electrons must have the range larger than CdTe film thickness and produce signal enhancement in CdTe. As this effect is observed at higher electron energies, the relative fractions of those electrons could be used for the signal increase estimate.

3 | RESULTS

This section contains results for backscattering electron spectra under a 6-MV photon beam, electron backscattering coefficients, modeled with monoenergetic electron sources, from metal back-reflectors, Cu or Pb, of various thicknesses, and backscattering data from combinations of CdTe with PMMA/Cu/Pb. The figures and tables show energies and thicknesses in units of keV and micrometers, respectively. In legends and other labels a number following each material represents its thickness.

3.1 | Secondary electrons generated under a 6-MV X-ray source

Detector structures of Figure 1 were first modeled with the 6-MV photon source to evaluate the overall effect of metal back-reflector on production and scattering of secondary (mostly through Compton effect) electrons traversing CdTe sensitive volume. Increase in the secondary electron fluence leads directly to the detector signal enhancement. Example of the change in the secondary electron fluence at the top and bottom surfaces of the sensitive volume of the basic structure (30-μm thick CdTe only) upon the addition of the metal layer in the modified designs is presented in Figure 3. Similar results were obtained for structures with 300-μm-thick CdTe layer.

Based on spectra shown here, the secondary electrons moving in the directions opposite to those of the source photons from the bottom surface of the detector can be drastically affected by the presence of the backscattering layer. Using Pb and Cu, the total fluence of electrons scattered back in CdTe with a metal back-reflector and CdTe alone were found to be increased by factors of 24 and 5, respectively. This suggests that the detector signal can be adjusted in a multilayered structure consisting of a sensitive volume and a metal back-reflector layer. For direct comparison, structures with equivalent thickness of CdTe were also simulated. Although the backscattered electron fluence with an additional Cu layer (CdTe30 + Cu20) is slightly lower than that with the additional CdTe layer of the same thickness (CdTe30 + CdTe20), the advantage of using metal instead of semiconductor is that the metal layer can serve as an electrode, thus allowing for lower bias applied across a thinner sensitive layer to achieve very similar signal.

The average energy of the electrons reflected from the bottom of CdTe was found to increase with the addition of a backscattering layer, especially for Pb, having the highest atomic number. Table 2 summarizes main characteristic parameters of fluence spectra in Figure 3, such as “backscattering” electrons fluence ratio (area under each graph in Figure 3, where CdTe30 structure is taken as unity) and deposited dose in CdTe volume. A dose ratio comparison among different configurations and CdTe only is also provided as an illustration of practically achievable signal enhancement.

The energy of the majority of generated secondary electrons is limited, becoming negligible above 1 MeV. As a result, we only focus on electrons up to 500 keV for basic CdTe and CdTe/Cu structures, extending it above 1 MeV only for CdTe/Pb configuration.

As the detector signal enhancement is primarily due to secondary electron backscattering from the back CdTe/metal layer, we next concentrate on electron transport properties in the basic and modified structures. We find it more straightforward and convenient to study that transport using the monoenergetic electron sources of radiation as described later.

3.2 | Electron backscattering coefficient

3.2.1 | Interactions of monoenergetic electrons in CdTe

We examined the change in backscattered and forward electron fluences at the correspondingly bottom and top surfaces of CdTe layer. MCNP simulations were used to calculate the energy spectra shown in Figure 4 for a film of 30-μm-thick CdTe. A good agreement for backscattering calculations using MCNP and EGSnrc for a 300-keV electron source is presented as an inset.

3.2.2 | Saturation thickness for a metal back-reflector

Electron backscattering is known to depend on the material thickness, reaching a bulk specimen value, known as the saturation thickness, when the layer thickness becomes about twice the electron range in the material. Figure 5 shows electron backscattering

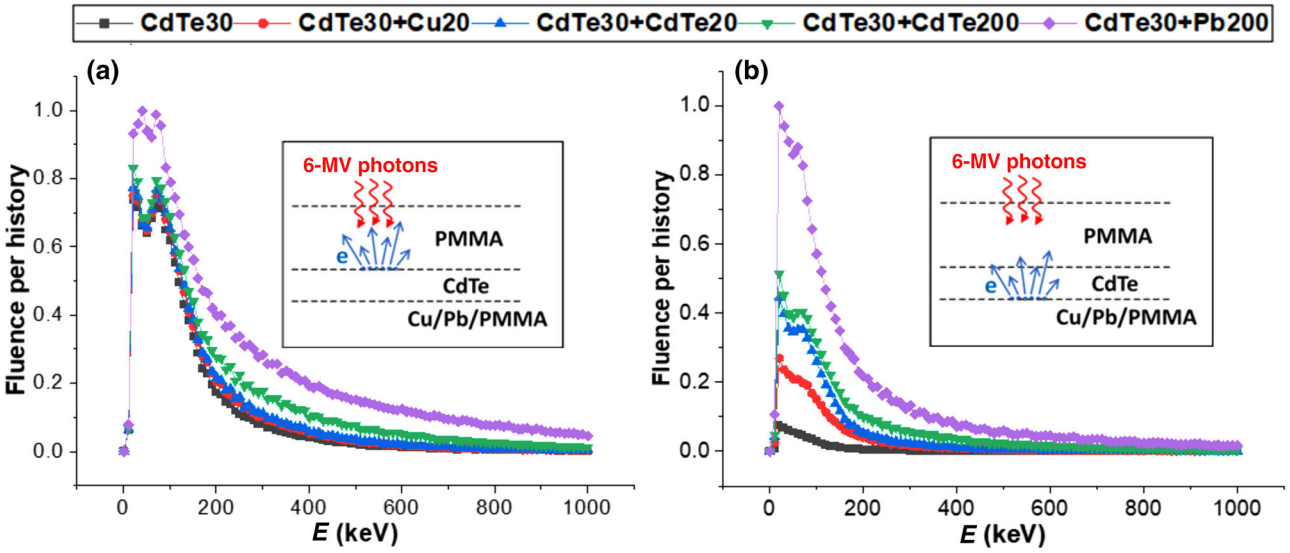

FIGURE 3 Fluence per history for the secondary electrons, generated under 6-MV photon beam and moving in the directions opposite to those of the source photons. (a) The spectra obtained at the top surface of the 30-μm-thick cadmium telluride (CdTe) detector, (b) the fluence spectra at the bottom surface of the 30-μm-thick CdTe detector-sensitive volume, and the modified structures using 20-μm Cu, 200-μm Pb, and additional CdTe layer of the 20-μm Cu and 200-μm thicknesses. The insets show sketches of simulation geometry.

TABLE 2 Summary of main characteristic parameters for electron fluence spectra of Figure 3 (all data obtained under 6-MV X-ray source)

	Fluence ratio			
Structure	Top surface of CdTe	Bottom surface of CdTe	Dose (MeV/g)	Dose ratio
CdTe30	1	1	8.50	1
CdTe30 + Cu20	1.11	5.04	9.20	1.08
CdTe30 + CdTe20	1.15	7.95	9.81	1.15
CdTe30 + CdTe200	1.45	11.54	10.82	1.27
CdTe30 + Pb200	2.17	24.42	14.80	1.74

Abbreviation: CdTe, cadmium telluride.

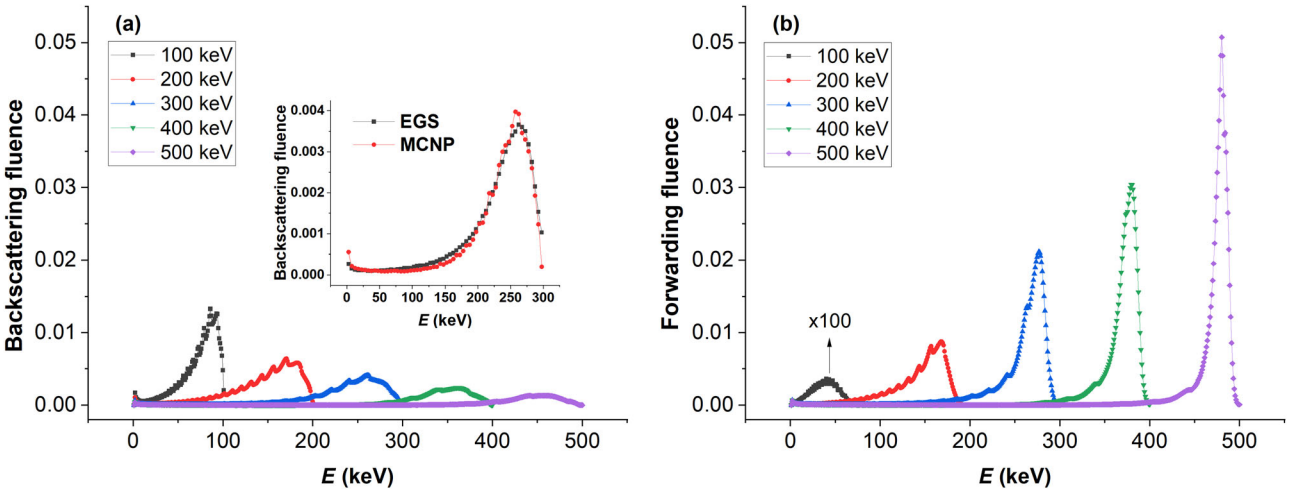

FIGURE 4 (a) Backscatter fluence spectra from a top surface of CdTe30, inset shows a side-by-side comparison of the backscatter fluence calculated by EGSnrc and MCNP codes for incident electrons of 300 keV. (b) Forward fluence at the bottom of CdTe30. The data from a 100-keV source is multiplied by 100.

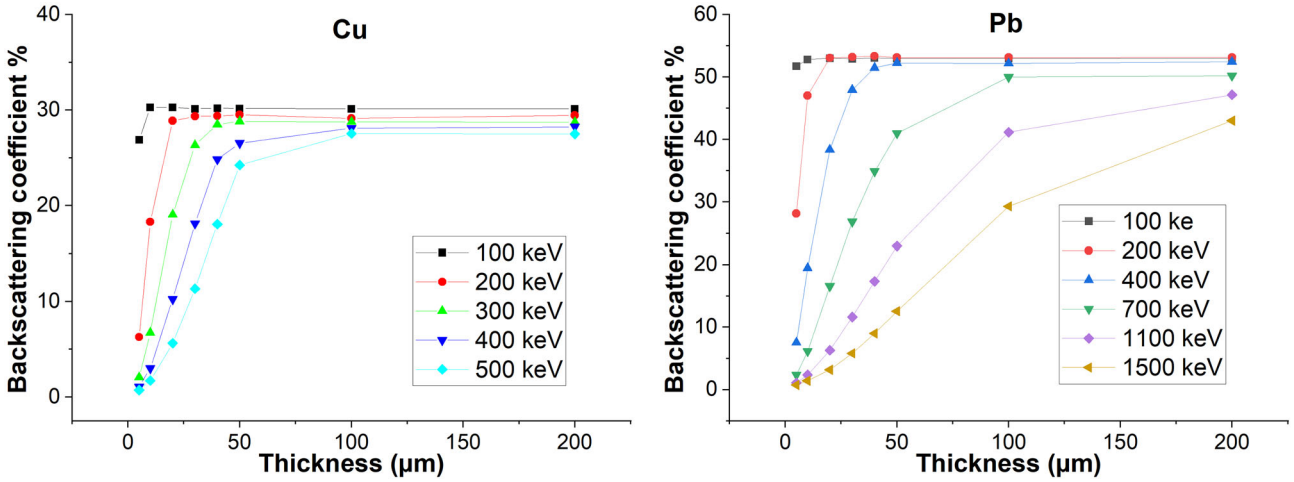

FIGURE 5 Backscattering coefficient versus thickness of metal back-reflectors of Cu and Pb

coefficient at Cu (Pb) and vacuum interface for varying film thickness and several electron source energies. The figure also illustrates differences among maximum backscattering from metals with a medium and high atomic numbers, Cu and Pb. Although these values were obtained with EGSnrc user code, a similar simulation for a subset of configurations using MCNP revealed good agreement, within 2%, in backscattering coefficient.

3.2.3 | Electron source energy dependence of the backscattering coefficient η

Although the main focus of this investigation is the effect of the back-reflector, we start with the evaluation of the omnipresent phantom-equivalent PMMA layer at the top of CdTe. Figure 6 shows the electron backscattering coefficient η as the function of the electron source energy for modified detector structures involving combinations of 30- and 300-μm-thick CdTe with PMMA (on top), and Cu and Pb (at the bottom) layers of varying thicknesses. Numbers in the legends represent the thickness in micrometers, for example, CdTe30 stands for CdTe only configuration, having a thickness of 30 μm, or PMMA1 + CdTe300 represents a structure with 1-μm-thick PMMA over 300-μm-thick CdTe. Symbols in Figure 6 show simulation results, in which the solid lines represent the best fits with the BiHill function,[35] which was utilized for all modeled structures.

Figure 6a,b shows that the addition of PMMA results in a reduction in η, more significant for the thinner CdTe. Figure 6c illustrates the electron backscattering coefficient for CdTe30 + Cu structure at various energies. Figure 6d, on the other hand, depicts a pattern that is consistent across all combinations indicating that the thick CdTe layer of 300 μm dominates the backscattering process for the relevant energy range. Figure 6e shows backscattering from CdTe and a high atomic number metal back-reflector of Pb over a wider range of energies. Figure 6f shows a pattern overall very similar to combination effects of thick CdTe and copper.

The maximum electron backscattering coefficient was found to be 44%, 42.7%, and 50% for 30-μm CdTe combinations with PMMA, Cu, and Pb, respectively. The position of the peak value shifts toward higher energies as the PMMA or metal thickness increases. When combined with PMMA, 300-μm CdTe has a maximum backscattering of 44%, whereas Cu and Pb both have a maximum backscattering of 42.7%. The modified structures of CdTe and underlying Cu or Pb metal back-reflectors produce different patterns of overlapped and split curves in the graphs.

The simulation results were fitted with BiHill function using Origin 9 software.[35] A basic description of these function properties and all fitting parameter values can be found in the Supporting Information section. Although the function has five fitting parameters, for most of the evaluated structures only two or three parameters were varied, the rest, describing the part of the graph with all curves collapsing on top of each other, were fixed. For all fits, *R*-square value of 0.98 or higher was achieved.

Another representation of the overall effect of combination of materials with significantly different atomic numbers is presented in Figure 7, using PMMA and CdTe for illustration. As evident from the figure, electron backscattering coefficients for the bilayered structures are limited among η-values of pure PMMA (the lowest curve) and pure CdTe (the highest curve). Electrons of low energies cannot reach the CdTe layer, and η reflects backscattering from the top layer only. For example, for a PMMA layer of 10-μm thickness, according to Table 1, a maximum range of low-energy electrons (below 20 keV) is 7 μm, which is not large enough for a backscattered electron to exit PMMA layer. As the energy increases above 50 keV, the range increases to at least four times greater than the PMMA thickness. Thus, electrons pass

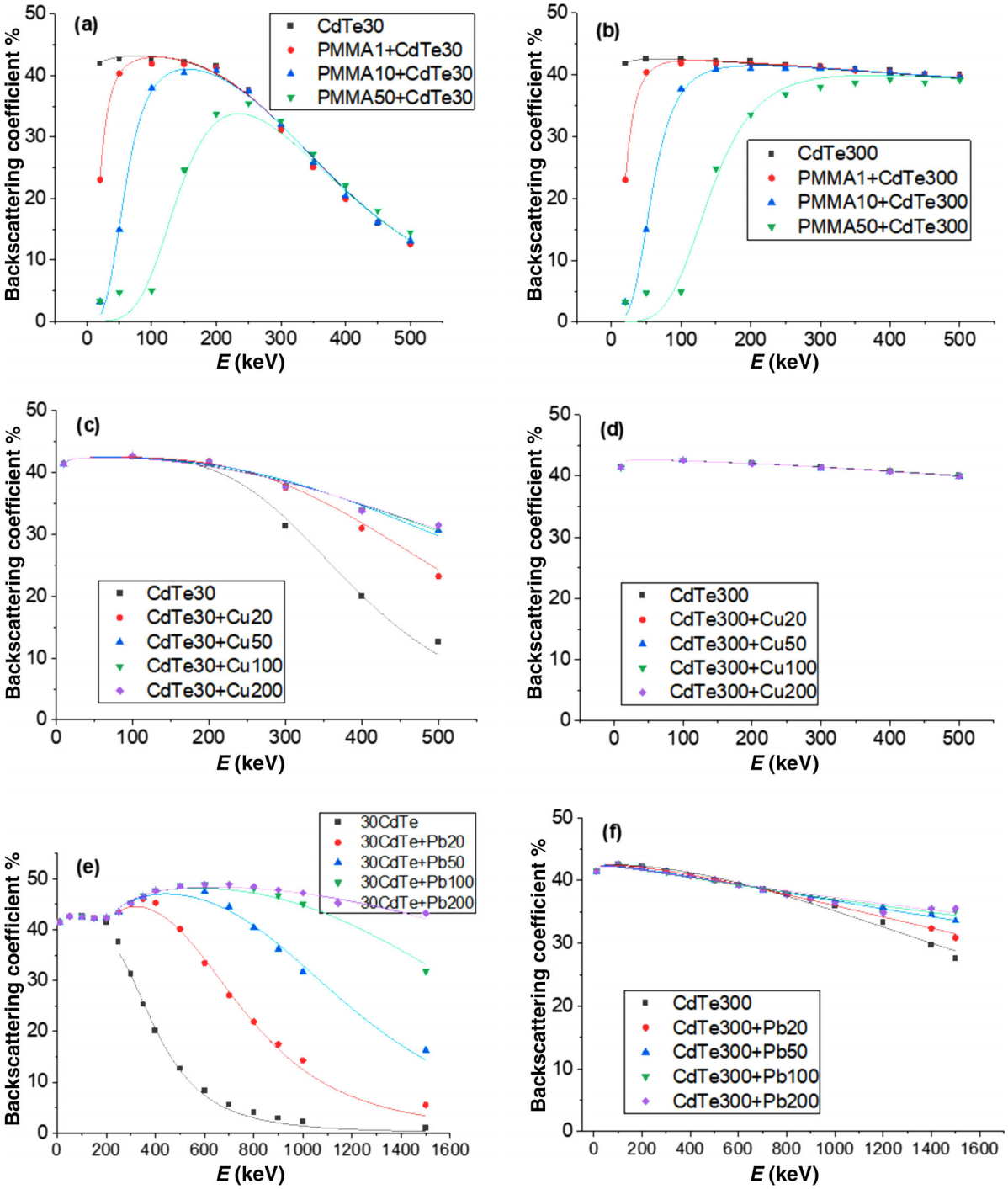

FIGURE 6 Electron backscattering coefficient (η) dependence on the electron source energy for various combinations of polymethyl methacrylate (PMMA) on top of cadmium telluride (CdTe), or Cu/Pb at the bottom of CdTe. Numbers in the legends represent thickness in micrometers; for example, CdTe30 stands for CdTe only configuration, having a thickness of 30 μm. Symbols show simulation results, and the solid lines represent the best fits with BiHill function (see the Supporting Information section). Parts (a, c, e) with 30-μm CdTe and (b, d, f) using 300-μm CdTe

through to the CdTe layer, and η increases toward the values of CdTe target. The trend of decreasing the backscattering coefficient for the low-energy electrons is independent of the CdTe thickness. The shape of the graphs in Figure 6a,b can be explained in a similar way.

3.2.4 | Backscattering coefficient data and signal enhancement

Here we will attempt to unify observations under 6-MV photon source in realistic detector structures (Figure 3) and the reflection coefficient results obtained under

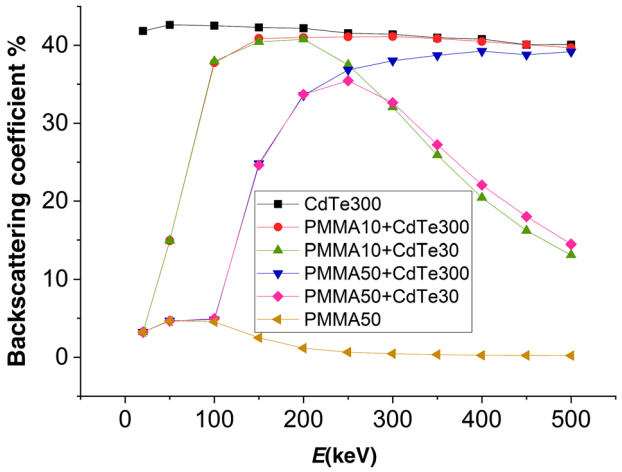

FIGURE 7 Backscattering coefficient versus energy of electron beam

electron sources. Generally speaking, the fluence of electrons moving toward the source (broadly named "backscattered") in Figure 3 from either top or bottom surface of CdTe may not be a good indicator of the dose deposition within the CdTe layer. The following two obvious factors complicate the relation between these parameters. (1) Due to the angular dependence, a substantial fraction of scattered electrons travel long distances in the lateral directions, some not even emerging from the CdTe layer. Although not adding to the electron fluence, they will nevertheless contribute to the energy deposition. (2) Fast electrons traverse CdTe film without much interaction; their fraction is relatively low, decreasing as $1/E^2$ with energy.[37] Such electrons will contribute more to the fluence count than to the dose, they emerge from the thin-film retaining most of their kinetic energy.

A detailed simulation of the energy deposition under the photon source shows indeed increase in the modified structures compared to the basic one of a single CdTe layer. Further analyzing the summary of simulation parameters presented in Table 2, we found a very strong correlation between the "backscattered" electron fluence ratios of Figure 3 and dose deposition. The corresponding plots are shown in Figure 8a,b for the fluence ratios for the top and bottom CdTe surfaces. In view of the previous factors, our established linear dependence between the fluences and doses appears rather nontrivial. It can perhaps be attributed to the mutual compensation of the earlier mentioned opposite trends in the simulated data where the fluences are integrated over the entire electron spectra. More discussion is provided in Section 4.

These considerations are conceptually similar to those obtained for the backscattering coefficient, showing increase in the η value for modified structures. As evident from Figure 6, the metal reflector contributes significantly to the backscattering coefficients of thinner, 30 μm, CdTe structures at higher energies. Above 300 keV, the η value increases by about 25% for CdTe/Cu, and by about 50% for CdTe/Pb, indicating proportional increase in high-energy backscattered electron fluence. At this energy, the electron range is much larger than the semiconductor thickness, allowing electrons reflected at various angles from the interface with metal (bottom of CdTe) traverse it another time, thus enhancing the energy deposition in CdTe. Plotting again a relationship between backscattered electron fluence ratio and the dose deposited in CdTe for the same configurations as considered in Figure 3, except with CdTe, or bilayer structures surrounded by vacuum, as for all the η value simulations, we also find linear dependence shown in Figure 8c. The electron source energy here was 300 keV, the dose deposited is much lower than in structures surrounded by the equilibrium layers of PMMA in photon simulations.

4 | DISCUSSION

In a detector under a megavoltage photon beam, the photons first transfer their energy to the electrons, mostly through the Compton effect. Set in motion, these electrons create electron–hole pairs that move to their respective terminals driven by the electric field (built-in or externally applied), thus forming the detector signal. Instead of a detailed simulation of the energy deposition in CdTe, we evaluated the behavior of the backscattering coefficients under a limited set of monoenergetic electron sources, utilizing available user code, which led to significantly shorter simulation times.

The materials investigated in this work represent those with very low, medium, and high atomic numbers Z, corresponding to PMMA, Cu/CdTe, and Pb. The high-Z targets exhibit stronger elastic scattering (proportional to Z^2), and correspondingly more significant deflections amplifying the yields of backscattered electrons. Another potentially important parameter is the ionization potential (I-value defined as the minimum energy required to eject an electron from an atomic shell), which increases from 74 eV for PMMA, to 823 eV for Pb; its energy loss dependence, however, is logarithmically weak. As a result, the approximate semiempirical Thomson–Whiddington energy loss relation holds[36]:

$$E_0^2 - E^2 = cL \tag{1}$$

where E_0 is the initial energy, E is the most probable energy of the electron that travel distance L, and c is a parameter that is proportional to Z and otherwise depends on the material parameters rather insignificantly.

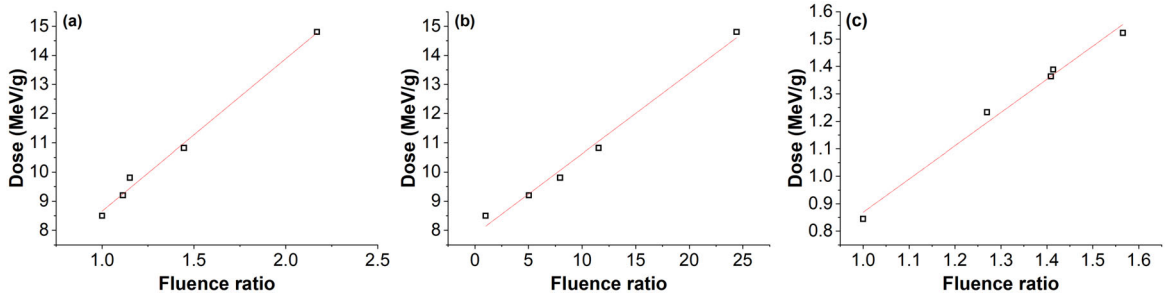

FIGURE 8 Relationship between the secondary electron fluence ratios and dose deposition in cadmium telluride (CdTe) layer obtained under 6-MV photon source (based on Figure 3 and Table 2) from the top (a) and the bottom (b) of CdTe layer. The data for 300-keV electron source (c) is shown for comparison. Solid lines represent linear fits.

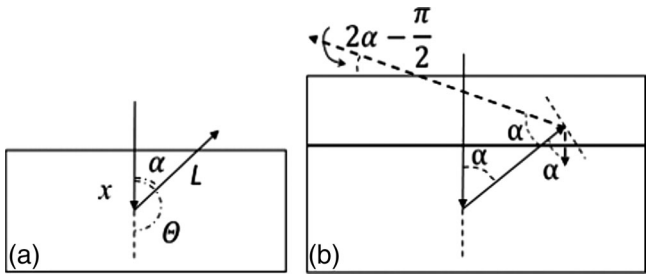

FIGURE 9 (a) Sketch of a single scattering event. Scattering angle α defines a scattering cone in 3D geometry. (b) Sketch of the scattering geometry for a bilayered structure

The latter dependence makes its imprint on the scattering cross section,

$$\frac{d\sigma}{d\Omega} = \frac{Z^2e^2}{4E^2}\frac{1}{(1+\cos\Theta)^2} = \frac{Z^2e^2}{4c}\frac{1}{R-L}\frac{1}{(1+\cos\Theta)^2} \tag{2}$$

where R is the electron range (determined from Equation (1) with $E = 0$), Ω is the solid angle, and Θ is the scattering angle illustrated in Figure 9a. The longer traveling distances decrease the electron energies and increase their scattering probabilities.

The distance L traveled by the backscattered electron is significantly larger than the scatterer depth x. Using Equation (2) the direct averaging of the complementary scattering angle α in Figure 9a yields $\langle\alpha\rangle = \int \alpha d\sigma / \int d\sigma \approx 70°$ and $L = x/\cos\alpha \approx 3x$. In addition, there is a significant dispersion of such angles, so some backscattered electrons travel distances exceeding the film thickness. Some of them do not escape the film, leading to the dose amplification.

If, on the other hand, the electron has enough energy to enter a tangent film on the top of the first one, as depicted in Figure 9b, then, upon the second scattering, (if takes place), its travel distance increases yet more, by a factor $\sim 1/\cos(2\langle\alpha\rangle - \frac{\pi}{2}) \approx 5$. It is then more likely for such an electron to slow down to the limit prohibiting its escape, which results in dose amplification.

The previous remarks allow one to understand the relevance of our used film thicknesses below the ranges for the electron energies of Table 1. For example, the 200-keV electron range of about 80 μm in Pb corresponds to the Pb layer thicknesses of about 20–30 μm in Figure 6c,e, according to the interpretation of Figure 9a. Similarly, if the top layer in Figure 9b represents CdTe, then the same energy of 200 keV would correspond to the film thickness of about 30 μm for CdTe in Figure 6a, and so on. All the graphs of Figure 6 can be interpreted along those lines. Our simulations in Figure 5 provide additional examples of electron ranges under large angles exceeding film thickness. For example, predicting relevant Cu film thickness of around 100 μm for the energy 500 keV nominally corresponds to the range of 300 μm, according to Table 1.

A similar analysis explains the role of the top PMMA layer used with some of our modeled structures. If the top layer in Figure 9b represents PMMA, which is almost "transparent" (in a sense of low scattering probability due to its low Z value), then about half of all the electrons are scattered back into the CdTe layer, hence a useful dose amplification effect in a semiconductor layer. Note, however, that PMMA layer can be responsible for lower backscattering count (and its related dose deposition in CdTe; cf. Figure 8) when its thickness (by itself or in combination with other layers) becomes sufficient to completely absorb the electrons, as is illustrated in Figure 6a. Figures 7 and 8 provide a more direct illustration of the latter statement. Note that in all the abovementioned figures, the decay on backscattering for high energies reflects a role of electrons penetrating through the entire structure and escaping detection.

We note that the previous sketches are based on a popular "single strong scattering" model neglecting possible diffusion propagation where electrons slow down enough to assume the more isotropic multiple scattering geometry. Taking the diffusion into account will result in certain quantitative changes, retaining, however, the previous qualitative conclusions.[3,6] In particular, the previous analysis provides qualitative insights into the nature of low-energy regions in Figures 3 and 4 as

attributed to long traveling distances for electrons with possible multiple scattering events.

We now touch upon the data of Figure 8. Its presented close-to-linear positive correlations between the "backscattering" electron fluence ratios and doses deposited in CdTe layer thus far appears to be a strong empirical observation, challenging the interpretation. According to Equation (2), the scattering cross section (translating into backscattering coefficient) varies as $1/E_0^2$. On the other hand, the stopping power is known to be inversely proportional to E_0. Therefore, the fluence of "backscattered" electrons will be proportional to their velocity, that is, $\sqrt{E} \approx \sqrt{E_0 - cL}$, making the composite dependence $E_0^{-2}\sqrt{E_0 - cL}$ somewhat closer to $1/E_0$. However, subsequent integration over travel paths along with empirical modifications of the stopping power[37] leaves too many unknowns. Therefore, we consider the observed linear dependencies of Figure 8 as empirical.

Overall, the results of this work show that adding metal back-reflectors of varied thickness below the sensitive volume of a detector would result in a greater signal, according to "backscattered" electron fluence illustrated in Figure 3. This suggests that dose to a detector can be adjusted in a multilayered structure. Figure 4 provides more information on the energy deposition and backscattering. In particular, the spectra's peak is relatively close to the source's energy, indicating that the spectra of a monoenergetic electron source are nearly unchanged.

5 | CONCLUSIONS

Although a very thin detector offers an extremely high resolution, desirable in some applications, it is limited by a low signal, often boosted with a top metal converter enhancing X-ray absorption. We proposed an extension of this approach with other functional layers in a detector structure. Two avenues had been explored: (1) adding a high-Z metal reflector layer to the back (instead of the typical front) detector surface, and (2) adding a top low-Z material to return to the detector layer its backscattered electrons (in a sense, functioning as a top film in the elimination optics). We have found that both approaches can provide noticeable improvements. In addition, we have attempted to relate the energy deposition in a semiconductor layer with the fluence of backscattered electrons that can often be obtained more easily. Backscattering coefficient calculation was found to be in good agreement between MCNP and EGSnrc codes. However, due to its convenience, EGSnrc user code was used to collect the majority of the data.

The present work is not limited to simply juxtaposing with standard detector structures: We have explored the issues of relevant energy spectra, backscattered fluences, and their correlations with the critical detector metric of dose deposition. Overall, our created picture appears self-consistent and useful for the future detector designs.

We have observed the following:

1. Low-energy components dominate the spectra of secondary and scattered electrons generated in thin films under high-energy X-ray sources.
2. The energy spectra of monoenergetic electrons backscattered by CdTe thin films spread extensively, demonstrating wide low-energy tails.
3. The thickness dependence of backscattering coefficients from thin films (studied in a wide range of parameters) exhibits saturations at values that very significantly exceed the electron ranges. That effect was shown to stem from the large-angle electron scattering.
4. The high-Z back layer (such as Pb) can increase the energy deposition by ~75% in the top semiconductor layer for the case of high-energy X-ray sources. When such a detector is used for high-energy electron source, the amplification may be much higher.
5. The low-Z top layer can be detrimental when its thickness is large enough. However, in practically implemental thicknesses of tens of micrometers its effect is positive due to partial electron reflection back to the semiconductor layer. This feature can be utilized with a thin PMMA layer inserted between a top metal plate and the semiconductor layer.
6. We have established a linear dependence between the energy deposition in a detector semiconductor layer and the backscattering coefficient of its related multilayer structure.
7. We have developed a qualitative understanding of the previous listed observations 1–6.

Practically speaking, we have developed an MC modeling approach for multilayered radiation detectors. Further studies along the lines of the methodology explored here are needed to quantify achievable signal enhancement for various thin films and other small sensitive volume detectors.

ACKNOWLEDGMENT

We are grateful to Dr. V. G. Karpov for useful discussions of physical aspects pertaining to this work.

CONFLICT OF INTEREST

The authors have no relevant conflicts of interest to disclose.

DATA AVAILABILITY STATEMENT

Authors will share data upon request to the corresponding author.

REFERENCES

1. Hegedus SS, Luque A. Status, trends, challenges and the bright future of solar electricity from photovoltaics. In: *Handbook of Photovoltaic Science and Engineering*. John Wiley & Sons; 2003:1-43.
2. Shvydka D, Parsai E, Kang J. Radiation hardness studies of CdTe thin films for clinical high-energy photon beam detectors. *Nucl Instrum Methods Phys Res A*. 2008;586(2):169-173.
3. Parsai EI, Shvydka D, Kang J. Design and optimization of large area thin-film CdTe detector for radiation therapy imaging applications. *Med Phys*. 2010;37(8):3980-3994.
4. Archard GD. Back scattering of electrons. *J Appl Phys*. 1961;32(8):6.
5. Dapor M. Backscattering of electrons from solid targets. *Phys Lett A*. 1990;151(1-2):84-89.
6. Drescher H, Krefting E, Reimer L, Seidel H. The orientation dependence of the electron backscattering coefficient of gold single crystal films. *Z Naturforsch A*. 1974;29(6):833-837.
7. Niedrig H. Physical background of electron backscattering. *Scanning*. 1978;1(1):17-34.
8. Dapor M. Role of the tail of high-energy secondary electrons in the Monte Carlo evaluation of the fraction of electrons backscattered from polymethylmethacrylate. *Appl Surf Sci*. 2017;391:3-11.
9. Dapor M. Theory of the interaction between an electron beam and a thin solid film. *Surf Sci*. 1992;269-270:753-762.
10. Wright KA, Trump JG. Back-scattering of megavolt electrons from thick targets. *J Appl Phys*. 1962;33(2): 687-690.
11. Kanter H. Backscattering of kilovolt electrons from thin films. *Br J Appl Phys*. 1964;15:6.
12. Dressel RW. Retrofugal electron flux from massive targets irradiated with a monoenergetic primary beam. *Phys Rev*. 1966;144(1):12.
13. Assa'd AMD, El Gomati MM. Backscattering coefficients for low energy electrons. *Scanning Microsc*. 1998;12(1):8.
14. Dapor M, Bazzanella N, Toniutti L, Miotello A, Gialanella S. Backscattered electrons from surface films deposited on bulk targets: a comparison between computational and experimental results. *Nucl Instrum Methods Phys Res, Sect B*. 2011;269:1672-1674.
15. Hussain A, Yang L, Mao S, Da B, Tőkési K, Ding Z. Determination of electron backscattering coefficient of beryllium by a high-precision Monte Carlo simulation. *Nucl Mater Energy*. 2021;26:100862.
16. Berger MJ. *Transmission and Reflection of Electrons by Aluminum Foils*. US Department of Commerce, National Bureau of Standards; 1963.
17. Martin J, Yuan J, Betancourt M, et al. New measurements and quantitative analysis of electron backscattering in the energy range of neutron β-decay. *Phys Rev C*. 2006;73(1):015501.
18. Kim SH, Pia MG, Basaglia T, et al. Validation test of Geant4 simulation of electron backscattering. *IEEE Trans Nucl Sci*. 2015;62(2):451-479.
19. Ali ESM, Rogers DWO. Benchmarking EGSnrc in the kilovoltage energy range against experimental measurements of charged particle backscatter coefficients. *Phys Med Biol*. 2008;53:18.
20. Jun Z, Liuxing H, Shengli N, Jinhui Z. Applications of Monte Carlo code to a study of low-energy electron backscattering from ultra-thin film on a substrate. International Conference on Mathematics and Computational Methods Applied to Nuclear Science and Engineering. 2011. ISBN 978-85-63688-00-2.
21. Dapor M. Backscattering of low energy electrons from carbon films deposited on aluminum: a Monte Carlo simulation. *J Appl Phys*. 2004;95(2):718-721.
22. Martin JW, Yuan J, Hoedl S, et al. Measurement of electron backscattering in the energy range of neutron β decay. *Phys Rev C*. 2003;68(5):055503.
23. Khan MA, Algarni H, Bouarissa N, Al-Hagan O, Alhuwaymel T. Composition dependence of penetration range and backscattering coefficient of electrons impinging on $SixGe_{1-x}$ and $GaAsxN_{1-x}$ semiconducting alloys. *Ultramicroscopy*. 2018;195:53-57.
24. Dapor M. Monte Carlo simulation of backscattered electrons and energy from thick targets and surface films. *Phys Rev B*. 1992;46(2):618.
25. Tan Z, Xia Y, Liu X, Zhao M. Monte-Carlo simulation of low-energy electron scattering in PMMA – using stopping powers from dielectric formalism. *Microelectron Eng*. 2005;77(3-4):285-291.
26. Yang L, Hussain A, Mao S, Da B, Tőkési K, Ding Z. Electron backscattering coefficients of molybdenum and tungsten based on the Monte Carlo simulations. *J Nucl Mater*. 2021;553:153042.
27. Frank L, Steklý R, Zadražil M, El-Gomati MM, Müllerová I. Electron backscattering from real and in-situ treated surfaces. *Microchim Acta*. 2000;132(2):179-188.
28. Assa'd A. Monte Carlo calculation of the backscattering coefficient of thin films of low on high atomic number materials and the reverse as a function of the incident electron energy and film thickness. *Appl Phys A*. 2018;124(10):1-6.
29. Kirihara Y, Namito Y, Iwase H, Hirayama H. Monte Carlo simulation of Tabata's electron backscattering experiments. *Nucl Instrum Methods Phys Res, Sect B*. 2010;268(15):2384-2390.
30. Ohya K. Secondary electron emission and backscattering from a metal surface under low-energy positron and electron bombardment. *Jpn J Appl Phys*. 1994;33(8R):4735.
31. Hussain A, Yang L, Zou Y, et al. Monte Carlo simulation study of electron yields from compound semiconductor materials. *J Appl Phys*. 2020;128(1):015305.
32. Roussillon Y, Karpov V, Shvydka D, Drayton J, Compaan A. Back contact and reach-through diode effects in thin-film photovoltaics. *J Appl Phys*. 2004;96(12):7283-7288.
33. Booth T. *A general Monte Carlo N-Particle Transport Code, Version 5, Volume 1: Overview and Theory*. Los Alamos National Laboratory; 2003.
34. Phase-space database for external beam radiotherapy. Accessed July 20, 2022. https://www-nds.iaea.org/phsp/photon/varian_truebeam_6mv
35. Ali ESM. *Making the EGSnrc/BEAMnrc System More Efficient, Accurate and Realistic in Simulating Kilovoltage X-Ray Systems*. Department of Physics Carleton University Ottawa-Carleton Institute of Physics Ottawa; 2007.
36. *OriginPro, Version 2021b. OriginLab Corporation, Northampton, MA, USA*. [computer program]. https://www.originlab.com
37. Dapor M. *Electron-Beam Interactions with Solids: Application of the Monte Carlo Method to Electron Scattering Problems*. Springer Berlin, Heidelberg; 2003.
38. Tan D, Heaton B. Simple empirical relations for electron CSDA range and electron energy loss. *Appl Radiat Isot*. 1994;45(4):527-528.

SUPPORTING INFORMATION

Additional supporting information can be found online in the Supporting Information section at the end of this article.

How to cite this article: Akbari F, Shvydka D. Electron backscattering for signal enhancement in a thin-film CdTe radiation detector. *Med Phys*. 2022;49:6654-6665.
https://doi.org/10.1002/mp.15813